International Journal of Pharmaceutics 427 (2012) 170–176

Contents lists available at SciVerse ScienceDirect

International Journal of Pharmaceutics

journal homepage: www.elsevier.com/locate/ijpharm

# Elastic–plastic contact law for simulation of tablet crushing using the biharmonic equation

Norhayati Ahmat*, Hassan Ugail[1], Gabriela González Castro[2]

*Centre for Visual Computing, University of Bradford, BD7 1DP, UK*

ARTICLE INFO

*Article history:*
Received 4 August 2011
Accepted 19 January 2012
Available online 2 February 2012

*Keywords:*
PDE method
Parametric surfaces
Contact law
Compression
Elastic–plastic deformation

ABSTRACT

This work presents a technique for shape modelling of cylindrical and spherical tablets subject to compression. This technique is based on the use of partial differential equations (PDEs), the biharmonic equation in particular. The deformation of the compressed elastic–plastic tablet of both shapes was obtained using the existing contact models found in literature. The mathematical properties of the biharmonic equation have been exploited to achieve simple mathematical expressions characterising the shape of the distorted tablet. Thus, the height, radius and contact area of both configurations due to uniaxial compression are represented by analytic expressions relating the coefficients associated with the solution of the biharmonic equation. The results obtained from the PDE-based simulation are compared with the theoretical ones. It is found that the analytic solution of the elliptic PDE can be utilised to represent the physical changes of the deformed object.

© 2012 Elsevier B.V. All rights reserved.

## 1. Introduction

In the pharmaceutical industry, tablets are produced by compacting powders or granules. Many tablets are often constituted by granules since they have better flow behaviour and can compress well even at a low pressure (Antonyuk et al., 2010). A granule is composed of several particles, which bond together by the adhesion force at the contact area (Antonyuk et al., 2005). A tablet formed from granules will have good characteristics such as consistent hardness, uniform content and ease of controlling drug release (Tousey, 2002).

The properties of tablets depend on the tabletting process and granule properties. The tabletting process, which involves three distinct stages (die filling, compaction process and ejection) can influence the mechanical strength of the tablet (Coube et al., 2005). It has been also shown that the bulk density of granules can affect the compression properties, in which low density granules give harder tablets (Spaniol et al., 2009). Furthermore, fast-dissolving tablets have been formed by high plastic granules which allow fast absorption of water into the compressed tablet and hence provide a soft paste for easy swallowing (Fu et al., 2005). This type of granule is produced by a wet granulation process and maintains its porosity even after it has been compressed as a tablet (Fu et al., 2005). Therefore, it is important to explore different formulations and techniques in order to obtain high-quality granular materials.

The Hertzian contact law has been widely used for a few decades in discrete element (Wellmann et al., 2008) and finite element (Kabir et al., 2008) simulations to study the flow and compression behaviours of elastic granules. Recently a new force–displacement model for an elastic–plastic granule has been developed (Antonyuk et al., 2010). This model is derived by extending the model of Tomas (2001) where the adhesion in the contact has been disregarded. Elastic and elastic–plastic laws are used in continuum mechanics studies since the properties of granules can be either elastic or elastic–plastic. Elasticity refers to the ability of a solid to recover its original shape and volume once the applied load is removed (Owolabi et al., 2010) whilst the plastic behaviour is in contrast to elastic behaviour. An elastic–plastic granule is a granule that has both the elastic and plastic properties. Therefore, it is necessary to understand the mechanical behaviour of granules at elastic, elastic–plastic and plastic range.

Many studies have been carried out to investigate the mechanical behaviour of elastic–plastic granules in compression tests by varying the size and shape of granules. For dry granular materials, their mechanical behaviour is measured using several methods such as ring-shear tests, grain characterisation and simple analogue experiments (Panien et al., 2006). On the other hand, the mechanical behaviour of wet granules need to be conducted numerically since they have more complicated behaviour compared to that of the dry granules (Schulz and Schulz, 2006). It has been reported in Herbold et al. (2008) that the crushing strength of the granule

* Corresponding author. Tel.: +44 7507262565.
*E-mail addresses:* n.b.ahmat@bradford.ac.uk (N. Ahmat), h.ugail@bradford.ac.uk (H. Ugail), g.gonzalezcastro1@bradford.ac.uk (G. González Castro).
[1] Tel.: +44 1274235464.
[2] Tel.: +44 1274233648.

0378-5173/$ – see front matter © 2012 Elsevier B.V. All rights reserved.
doi:10.1016/j.ijpharm.2012.01.053

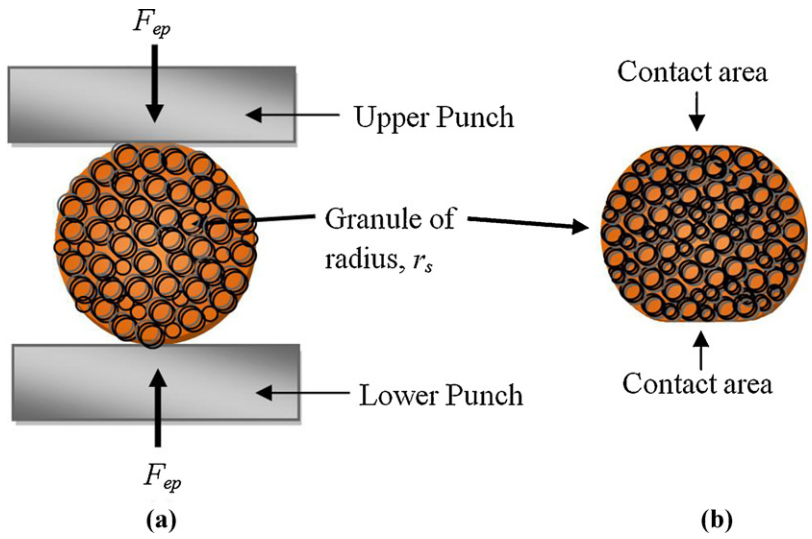


**Fig. 1.** Compression of a spherical granule. (a) The slow compression of a spherical granule with two contact points. (b) The shape of a granule after the elastic–plastic deformation.

decreases as the granule size increases. Furthermore, researchers have shown that a spherical granule has lower flow stresses than the non-spherical counterpart (Iveson and Page, 2005). Furthermore, according to them, both shapes exhibited transformation from brittle to plastic failure during the uniaxial compression test.

The purpose of this work is to use PDEs as the foundation for modelling the mechanical behaviour of compressed cylindrical and spherical tablets. Generally, the shape of tablets is a cylinder or oval. However, in this present work we generated a PDE-based representation of a spherical-shaped tablet and assumed the mechanical behaviour of the tablet with that particular shape is similar to the behaviour of a spherical granule. Therefore, we have made use of the contact law of a granule found in literature to measure the displacement of a compressed spherical tablet and hence relating the physics of the law to the parametric shape relating to the tablet in question.

The biharmonic equation has been applied to many areas of computer graphics including 3D data modelling and processing, surface blending (You et al., 2004) and animation (González Castro et al., 2010). This method can generate a smooth surface from a set of boundary curves with a small number of design parameters. Several surface patches can be blended together in order to model a complex geometry. Moreover, PDE surfaces can easily be manipulated and remain continuous when the values of its design parameters are changed (Ugail, 2004). In this context, PDE-based representations of an object can adapt to physical changes when the compression test takes place.

The rest of this paper is organised as follows. Section 2 describes the contact models for elastic–plastic tablets and granules by slow compression. Section 3 provides a brief description on the modelling technique for generating the shape of the compressed cylindrical and spherical tablets. Section 4 discusses the theoretical and PDE-based results for compressed tablets in both shapes. Finally, Section 5 presents the conclusions of this work.

## 2. Elastic–plastic contact deformation

In this section, we discuss the mechanical behaviour of two different objects, a cylindrical tablet and a spherical granule, under a uniaxial compression. It is assumed that both the tablet and the granule are homogeneous and isotropic.

Recently, a force–displacement model of an axially compressed flat-faced cylindrical tablet has been proposed by Ahmat et al. (2010),

$$\omega_z = \omega_{z0} + \frac{100Fz^2(1+\gamma)}{AhE}\left[\frac{z^2\gamma}{r^2} - \frac{1-\gamma}{2} + \frac{\gamma^2}{\gamma-1}\left(1-\frac{c^2}{r^2}\right)\right], \quad r > 0, \tag{1}$$

where $A$, $c$ and $h$ are the contact area, radius and initial height of the tablet respectively, $\omega_{z0}$ represents an adjustment constant, $F$ denotes the axial force, $E$ is the Young's modulus, $\gamma$ is the Poisson ratio whilst $z$ and $r$ are any point in axial and radial directions respectively. The model was developed by utilising one of the solutions of the Love's stress function together with a particular set of boundary conditions. The reader can find further details of this model in the work presented by Ahmat et al. (2010).

In the case of granules, when a soft spherical granule is compressed by two flat surface punches, as shown in Fig. 1(a), two contact areas are formed. The contact area deforms as a circle with radius, $r_c$ which depends on the granule radius, $r_s$. According to the existing literature, the radius of the contact area is smaller than the deformed area (Antonyuk et al., 2010). The shape of the

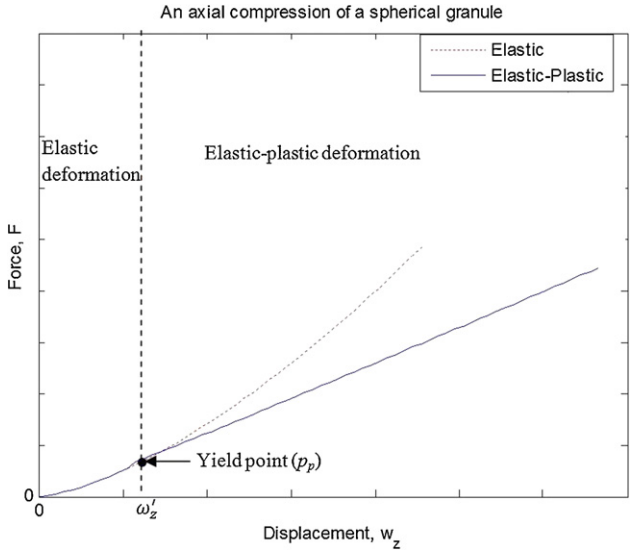


**Fig. 2.** Force–displacement curve of a spherical granule during the compression test. This graph has been reproduced from Antonyuk et al. (2010).

compressed granule is illustrated in Fig. 1(b) where the small spheres in the granule (before and after compression) represent the group of powder particles.

For an elastic–plastic granule, the plastic deformation starts when the pressure reaches the micro-yield strength, $s_y$. However, some authors have reported that the plastic deformation begins when the maximum contact pressure reaches at 1.6 times of the uniaxial yield stress (Li et al., 2009). Before the yield point ($p_p$) is reached, the force–displacement curve of the loaded spherical granule shows a nonlinear elastic deformation which follows Hertz law (Tomas, 2001),

$$F_e = \frac{E}{3(1-\gamma^2)}\sqrt{2r_s\omega_z^3}, \tag{2}$$

where $\omega_z$ is the full axial displacement. The material behaviour changes from elastic to elastic–plastic at the yield point as shown in Fig. 2. When the pressure exceeded the yield pressure ($P_y$), the total axial displacement of the compressed elastic–plastic granule at force, $F_{ep}$ is given by (Antonyuk et al., 2010),

$$\omega_z = \frac{1}{81r_s s_y}\left[\frac{J^{1/3}}{\pi} + \frac{\omega_z' s_y r_s(\omega_z'\pi s_y r_s + 324F_{ep})}{J^{1/3}} + \frac{\omega_z'\pi s_y r_s + 162F_{ep}}{\pi}\right], \tag{3}$$

where

$$J = \omega'_z\pi s_y r_s\left(1458F_{ep}\sqrt{F_{ep}(2\omega_z'\pi s_y r_s + 729F_{ep})} + 39,366F_{ep}^2 + (\omega_z'\pi s_y r_s)^2 + 486\omega_z'\pi s_y r_s F_{ep}\right), \tag{4}$$

and $\omega_z'$ is the displacement at the yield point and the micro-yield strength can be derived as

$$s_y = \frac{2E}{\pi(1-\gamma^2)}\sqrt{\frac{\omega_z'}{r_s}}. \tag{5}$$

Furthermore, the radius of the contact area of the granule during the elastic–plastic deformation is given by,

$$r_c = \sqrt{r_s\omega_z}. \tag{6}$$

In this work, the linear elastic–plastic models proposed by Ahmat et al. (2010) and Antonyuk et al. (2010) will be used to measure the axial displacement of axially compressed cylindrical and spherical tablets respectively. The theoretical results obtained from these models will be compared with the simulation results generated from the PDE method.

## 3. PDEs for shape modelling

In this section, we provide the essential information concerning the theoretical modelling of our shape parameterisation technique. The geometry of the objects in this work are designed by employing the solution to the biharmonic equation given by,

$$\left(\frac{\partial^2}{\partial u^2} + \frac{\partial^2}{\partial v^2}\right)^2 \underline{\chi}(u,v) = 0, \tag{7}$$

where $\underline{\chi}(u,v)$ represents the parametric 3D surface in domain $u$ and $v$ where $0 \le u \le 1$ and $0 \le v \le 2\pi$. The details on the complete solution of Eq. (7) can be found in the work presented by Bloor and Wilson (1989), which initially introduced the PDE method into the area of blend-shape generation in computer-aided design (CAD). The analytic solution of Eq. (7) is found using the separation of variables method together with a set of periodic boundary conditions and can be written as,

$$\underline{\chi}(u,v) = \underline{A}_0 + \sum_{n=1}^{\infty}[\underline{A}_n(u)\cos(nv) + \underline{B}_n(u)\sin(nv)], \tag{8}$$

which can be approximated to a finite value $N$ as,

$$\underline{\chi}(u,v) = \underline{A}_0 + \sum_{n=1}^{N}[\underline{A}_n(u)\cos(nv) + \underline{B}_n(u)\sin(nv)] + \underline{R}(u,v), \tag{9}$$

where

$$\underline{A}_0 = \sum_{m=0}^{3}\underline{a}_{0m}u^m, \tag{10}$$

$$\underline{A}_n = (\underline{a}_{n1} + \underline{a}_{n3}u)e^{nu} + (\underline{a}_{n2} + \underline{a}_{n4}u)e^{-nu}, \tag{11}$$

$$\underline{B}_n = (\underline{b}_{n1} + \underline{b}_{n3}u)e^{nu} + (\underline{b}_{n2} + \underline{b}_{n4}u)e^{-nu}, \tag{12}$$

$$\underline{R}(u,v) = (\underline{r}_1(v) + \underline{r}_3(v)u)e^{\beta u} + (\underline{r}_2(v) + \underline{r}_4(v)u)e^{-\beta u}. \tag{13}$$

The term $\underline{A}_0$ defines the spine of the surface patch that brings out the symmetries of that patch whilst $\sum_{n=1}^{\infty}[\underline{A}_n\cos(nv) + \underline{B}_n\sin(nv)]$ gives a radial position of a point on the surface patch away from the spine and $\underline{R}$ is a remainder function responsible for exactly satisfying the original boundary conditions (Ugail, 2004). The vector-valued constants $\underline{a}_{0m}$, $\underline{a}_{ni}$ and $\underline{b}_{ni}$ are determined by the specified boundary conditions, $\underline{r}_i$ is obtained from the difference between the original boundary conditions and the approximated ones whilst the value of $\beta$ is chosen as $N+1$.

Fig. 3 presents the resulting shape of the PDE surface generated using 4 curves in the 3-space. These rectangular-shaped curves have been used as the boundary conditions to solve the biharmonic equation. The PDE surface in Fig. 3 is generated by truncating the expansion after 5 modes. It is worth highlighting that the shape of the patch can be controlled solely by the shape of its boundary curves.

The spine of an object possesses many geometric properties, one of which is that it constitutes the medial axis (or skeleton) of the shape. Furthermore, the spine also represents more topologies than that of the object it is obtained from (Ugail, 2004). Some notable work has been carried out to investigate how the spine of the PDE surface can be utilised in parameterising complex shapes (Ugail, 2004). In that work, the author has shown that the spine of the PDE surface can be used as a powerful tool for shape manipulation. Furthermore, a cyclic animation has been achieved by exploiting the mathematical expression associated with the spine of the PDE surface as a driving mechanism (González Castro et al., 2010).

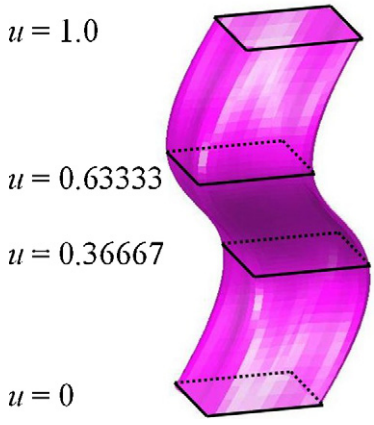


**Fig. 3.** Shape of the PDE surface subject to the particular boundary conditions.

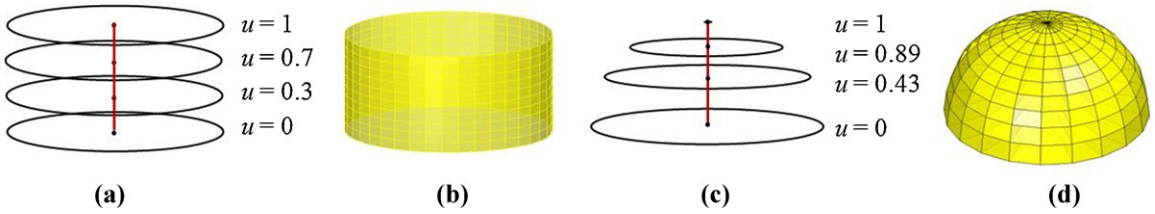


**Fig. 4.** Generating curves for a cylinder and hemisphere in (a) and (c). The spine of each surface is also outlined. The resulting surface shape of a cylinder and a hemisphere in (b) and (d) respectively.

In order to study the mechanical behaviour of the compressed cylindrical and spherical tablets using the PDE method, first we need to create the boundary curves that will describe the geometry shape of both objects as can be seen in Fig. 4(a) and (b). For the spherical-shaped tablet, only the boundary curves of a hemisphere are created because of the geometrical and loading symmetries. These curves are saved in external .OBJ files. Next, we implemented the PDE method in a C++ program to read the boundary curves and produce the solution for each set of curves. Finally, the PDE surface is generated from these boundary curves. For instance, Fig. 4(d) shows the generated PDE-based representation of a hemisphere which has been obtained using a mesh grid 11 by 21 points.

Given that the above formulation of the PDE method only generates the surface of any given object, a new parameter, $w$ in domain $0 \le w \le 1$ has been introduced into Eq. (8) in order to generate a solid representation of that particular object (Ahmat et al., 2010). This leads to,

$$\underline{\chi}(u, v) = \underline{A}_0 + w\sum_{n=1}^{\infty}[\underline{A}_n(u)\cos(nv) + \underline{B}_n(u)\sin(nv)]. \quad (14)$$

This parameter generates interior points of the PDE-based object from the spine towards its surface. The solid shape of the cylinder and hemisphere have been generated and are shown in Fig. 5. In that figure, the parametric region is set as $0 \le (u,w) \le 1$ and $(\pi/2) \le v \le 2\pi$.

In order to find the contact radius and height of the cylinder and sphere when they have been compressed axially, we need to exploit the mathematical properties associated with the analytic

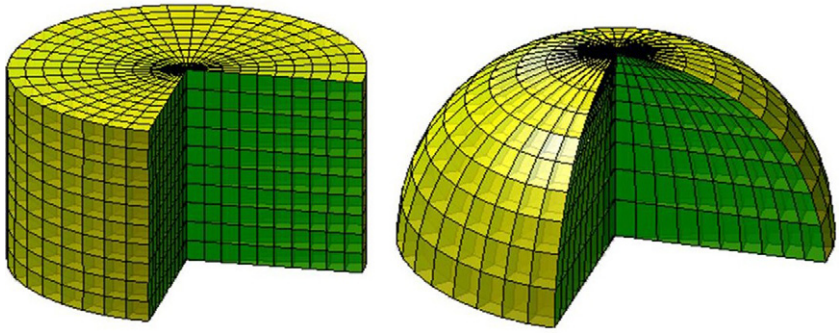

**Fig. 5.** Solid PDE-based representation of cylindrical and hemispherical tablets.

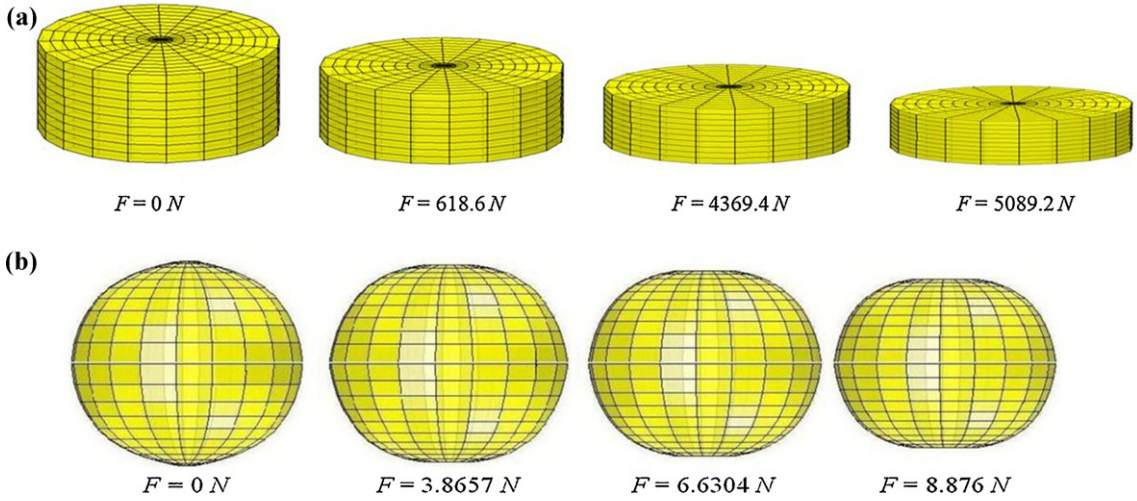


**Fig. 6.** Solid PDE-based representation of a compressed cylindrical and spherical tablets in (a) and (b) respectively.

solution of the PDE (Eq. (14)) which can be written of the form,

$$(\chi_x, \chi_y, \chi_z) = \begin{pmatrix} A_{0x} + w\sum_{n=1}^{N}[A_{nx}\cos(nv) + B_{nx}\sin(nv)] + R_x, \\ A_{0y} + w\sum_{n=1}^{N}[A_{ny}\cos(nv) + B_{ny}\sin(nv)] + R_y, \\ A_{0z} + w\sum_{n=1}^{N}[A_{nz}\cos(nv) + B_{nz}\sin(nv)] + R_z \end{pmatrix}. \quad (15)$$

Given that the boundary curves of the cylinder and sphere represent circles, the approximated solution of the elliptic PDE fits the original boundary conditions perfectly. Hence, the vector $\underline{R}$ is equal to zero. Thus, only the term $\underline{A}_0$ and the finite series in Eq. (15) can be considered to represent the height and contact radius of both objects respectively.

The parametric form of a circle with centre coordinates ($x_0$, $y_0$, $z$) and radius, $r$ are written as,

$$(x, y, z) = (x_0 + r\cos v, y_0 + r\sin v, z). \quad (16)$$

By comparing Eqs. (15) and (16), the centre coordinate of the boundary curve is ($A_{0x}$, $A_{0y}$, $A_{0z}$). As one can see in Fig. 4(a) and (b), the spine of the cylinder and sphere is a straight line parallel to $z$, therefore only $A_{0z}$ is used to represent the spine of both objects,

$$A_{0z} = a_{00z} + a_{01z}u. \quad (17)$$

Next, we use the analytic expression for the radius associated with the PDE surface to find the relation between $\underline{A}_n$ and $\underline{B}_n$, and thus obtaining the simplified equation of the radius. By simple comparison between Eqs. (15) and (16) when $w = 1$, we noticed that,

$$r\cos(v) = \sum_{n=1}^{N}[A_{nx}\cos(nv) + B_{nx}\sin(nv)] = A_{1x}\cos(v) + B_{1x}\sin(v) + A_{2x}\cos(2v) + B_{2x}\sin(2v) + \cdots + A_{Nx}\cos(Nv) + B_{Nx}\sin(Nv) \quad (18)$$

and

$$r\sin(v) = \sum_{n=1}^{N}[A_{ny}\cos(nv) + B_{ny}\sin(nv)] = A_{1y}\cos(v) + B_{1y}\sin(v) + A_{2y}\cos(2v) + B_{2y}\sin(2v) + \cdots + A_{Ny}\cos(Nv) + B_{Ny}\sin(Nv) \quad (19)$$

From Eqs. (18) and (19), we can see that $A_{nx}$, $B_{nx}$, $A_{ny}$ and $B_{ny}$ for $n > 1$ are zero. Thus, we can rewrite Eqs. (18) and (19) as,

$$r\cos(v) = A_{1x}\cos(v) + B_{1x}\sin(v) \quad \text{and}$$
$$r\sin(v) = A_{1y}\cos(v) + B_{1y}\sin(v). \quad (20)$$

As a result, it is observed that $A_{1x} = B_{1y}$. Another relationship can be found from the basic equation of a circle,

$$r^2 = x^2 + y^2 = (r\cos v)^2 + (r\sin v)^2, \quad (21)$$

where we substitute Eq. (20) into Eq. (21),

$$(r\cos v)^2 + (r\sin v)^2 = (A_{1x}\cos(v) + B_{1x}\sin(v))^2 + (A_{1y}\cos(v) + B_{1y}\sin(v))^2,$$
$$r^2(\cos v)^2 + r^2(\sin v)^2 = (A_{1x}^2 + A_{1y}^2)(\cos v)^2 + (B_{1x}^2 + B_{1y}^2)(\sin v)^2 + 2(A_{1x}B_{1x} + A_{1y}B_{1y})\sin v\cos v. \quad (22)$$

By comparing the LHS and RHS of Eq. (22), the radius of both objects is then given by,

$$r = \sqrt{A_{1x}^2 + A_{1y}^2} = \sqrt{B_{1x}^2 + B_{1y}^2}, \quad (23)$$

and therefore,

$$A_{1y} = -B_{1x}. \quad (24)$$

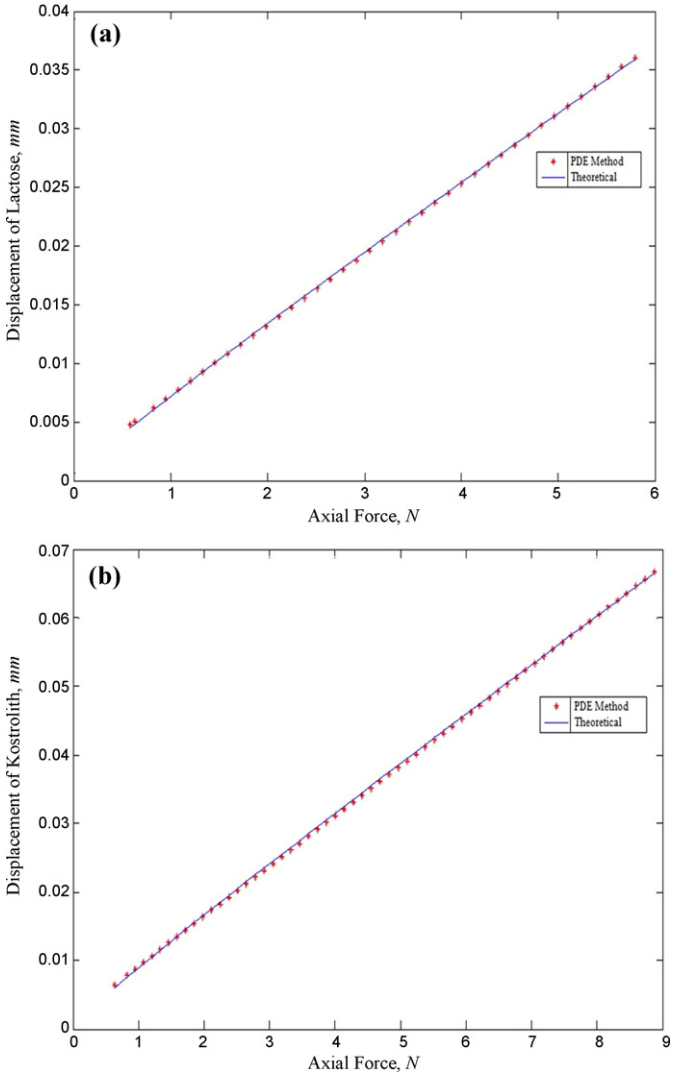


**Fig. 7.** Theoretical and PDE-based force–displacement relationships for the compressed spherical (a) lactose and (b) Köstrolith.

The height of the PDE-based sphere or cylinder can be measured from the length of the spine,

$$h = A_{0z}(u = 1) - A_{0z}(u = 0) = a_{01z}, \quad (25)$$

whilst the contact radius is given as,

$$r_c = \sqrt{(A_{1x}(u = 1))^2 + (A_{1y}(u = 1))^2}. \quad (26)$$

Therefore, it is important to stress that Eqs. (25) and (26) can be used for the simulation corresponding to the height and contact area of the PDE-based representation of the pharmaceutical objects respectively.

## 4. Results and discussion

Simulations of the compressed cylindrical and spherical tablets have been carried out on two different elastic–plastic industrial materials. The details of corresponding material properties are found from the literature and are listed in Table 1.

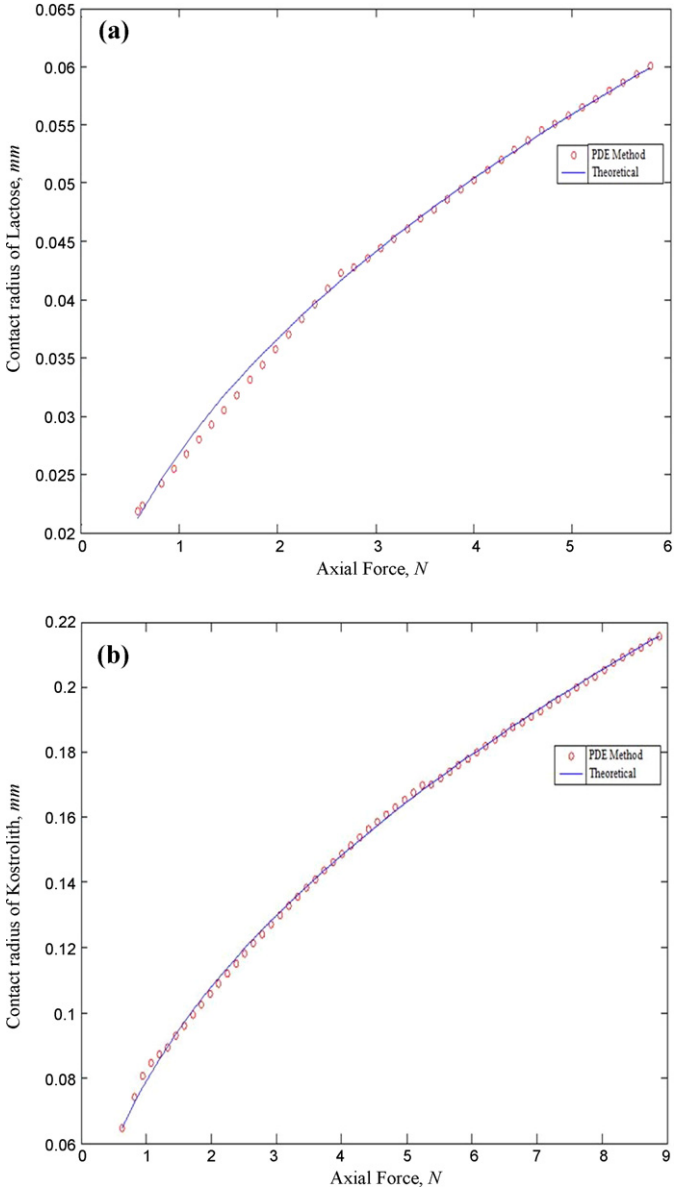


**Fig. 8.** Comparison between the radius of contact area of the theoretical and PDE-based spherical (a) lactose and (b) Köstrolith.

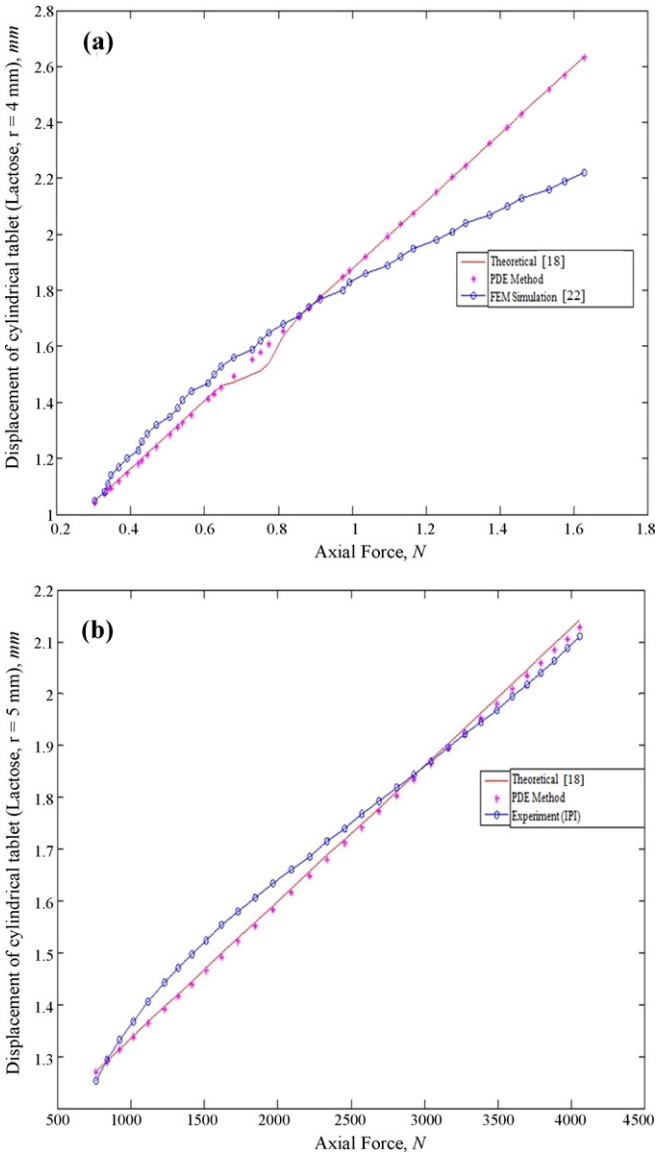


**Fig. 9.** (a) FEM versus PDE simulations force–displacement curves. (b) Comparison between the displacement of experimental and simulated compression on lactose powder.

The shapes of the solid PDE-based representation of a cylindrical lactose tablet and a spherical Köstrolith tablet at different forces are illustrated in Fig. 6. It is assumed that the contact between the pharmaceutical tablet and the punches is frictionless. The generated objects consists of 2000 cuboids, which is produced by defining the parameter $u$ and $w$ from 0 to 1 and divided it into 10 equal parts whilst parameter $v$ is defined by $0, \pi/10, \pi/5, \ldots, 2\pi$.

Fig. 7 shows the contact force–displacement graphs of two different materials in a spherical shaped configuration, which is defined by Eqs. (3) and (25). Given that our work focuses on the elastic–plastic deformation behaviour, both graphs start after the load reaches the yield point. A striking linear relationship between the displacements and the force is observed. Since the force–displacement model (Eq. (3)) is employed to the boundary curve of the sphere, hence it is found that our simulation results agree with the analytical expression remarkably well.

The comparison between the theoretical and simulated contact radius as a function of the axial force have been shown in Fig. 8. It is observed that the contact radius of spherical lactose and Köstrolith measured by Eq. (6) are slightly different from those generated by Eq. (26) at the lower forces. However, as the contact

**Table 1**
Mechanical characteristics of the examined materials by compression.

| Material | Shape | Radius (mm) | $E$ (N/mm$^2$) | $\gamma$ | $S_y$ (N/mm$^2$) |
|---|---|---|---|---|---|
| Lactose (Wu et al., 2003) | Sphere | 0.1 | 2080 | 0.30 | 616.6 |
| Köstrolith (Antonyuk et al., 2005) | Sphere | 0.7 | 820 | 0.28 | 71.007 |
| Lactose (Wu et al., 2008) | Cylinder | 4.0 | 3570 | 0.12 | 222.22 |
| Lactose (Ahmat et al., 2010) | Cylinder | 5.0 | 2640 | 0.21 | 34.013 |

force is increased, the curve generated by the PDE method fitted the theoretical ones.

Fig. 9 displays the force–displacement graphs of compressed cylindrical tablets consisting of lactose with different properties (refer Table 1). The force–displacement curve of a tablet with radius 4 mm which is obtained from the Finite Element Method (FEM) simulation (Wu et al., 2008) shown in Fig. 9(a) is clearly convex. In contrast, for the PDE simulation which applies Eq. (1), there is a linear relationship between the axial force and normal displacement. This difference occurs because the result from FEM simulation is obtained numerically whilst the other one has been found analytically. Moreover, the result of the PDE-based models is sensitive to the elastic properties of the material (Ahmat et al., 2010). On the other hand, a good agreement between the experimental and simulation results in Fig. 9(b) shows the good accuracy of the PDE-based model. The experimental result of a compressed cylindrical tablet of radius 5 mm was produced by the Institute of Pharmaceutical Innovation (IPI), University of Bradford.

It is clear that the results for the compressed PDE-based representation of cylindrical and spherical tablets are in close agreement with the elastic–plastic deformation models proposed in the literature. From all our results, it seems that the solution associated with the particular PDE representing the shape of the tablets under axial compression can be related to the existing contact law models and defined key parameters of the overall shape to the PDE coefficients. Another interesting observation in our results is that the height and contact radius of the deformed PDE-based representation of a spherical tablet can be generated by a small set of parameters.

## 5. Conclusions

The work presented in this paper focuses on the application of the PDE method for designing a parametric representation of deformed pharmaceutical tablets in cylindrical and spherical shapes. The PDE surfaces are generated from boundary curves and a small set of design parameters. This method can be easily adopted by taking advantage of its mathematical properties. The various case studies presented in this paper show that the solution to a particular elliptic PDE can be exploited as a tool for representing the deformation and contact law for elastic–plastic cylindrical and spherical tablets. This is due to the fact that the spine and radius of the PDE-based object are determined analytically.

The PDE-based simulations of a compressed elastic–plastic cylinder and sphere are also discussed. The simulation results show a very good agreement with the elastic–plastic models of both objects found in literature. However, this simulation can only be applied to the case involving axial compression of an object generated from circular-shaped boundary curves and future work can be carried out to generalise this to more general boundary conditions.

## Acknowledgements

The authors acknowledge Ministry of Higher Education Malaysia and University Pendidikan Sultan Idris (UPSI) for financial sponsorship to N. Ahmat.

## References

Ahmat, N., Ugail, H., González Castro, G., 2010. Method of modelling the compaction behaviour of cylindrical pharmaceutical tablets. Int. J. Pharm. 405, 113–121.
Antonyuk, S., Heinrich, S., Tomas, J., Deen, N.G., Van Buijtenen, M.S., Kuipers, J.A.M., 2010. Energy absorption during compression and impact of dry elastic–plastic spherical granules. Granular Matter 12, 15–47.
Antonyuk, S., Tomas, J., Heinrich, S., Mörl, L., 2005. Breakage behaviour of spherical granulates by compression. Chem. Eng. Sci. 60, 4031–4044.
Bloor, M.I.G., Wilson, M.J., 1989. Generating blend surfaces using partial differential equations. Comput. Aided Des. 21, 165–171.
Coube, O., Cocks, A.C.F., Wu, C.Y., 2005. Experimental and numerical study of die filling, powder transfer and die compaction. Powder Metall. 48, 68–76.
Fu, Y., Jeong, S.H., Park, K., 2005. Fast-melting tablets based on highly plastic granules. J. Control. Release 109, 203–210.
González Castro, G., Athanasopoulos, M., Ugail, H., 2010. Cyclic animation using partial differential equations. Vis. Comput. 26, 325–338.
Herbold, E.B., Nesterenko, V.F., Benson, D.J., Cai, J., Vecchio, K.S., Jiang, F., Addiss, J.W., Walley, S.M., Proud, W.G., 2008. Particle size effect on strength, failure, and shock behavior in pol-tetrafluoro-ethylene-Al–W granular composite materials. J. Appl. Phys. 104, article 103903.
Iveson, S.M., Page, N.W., 2005. Dynamic strength of liquid-bound granular materials: the effect of particle size and shape. Powder Technol. 152, 79–89.
Kabir, M., Lovell, M., Higgs, C., 2008. Utilizing the explicit finite element method for studying granular flows. Tribol. Lett. 29, 85–94.
Li, F., Pan, J., Sinka, C., 2009. Contact laws between solid particles. J. Mech. Phys. Solids 57, 1194–1208.
Owolabi, B.I.O., Afolabi, T.A., Adebowale, K.O., 2010. Effect of heat moisture treatment on the functional and tabletting properties of corn starch. Afr. J. Pharm. Pharmacol. 4, 498–510.
Panien, M., Schreurs, G., Pfiffner, A., 2006. Mechanical behaviour of granular materials used in analogue modelling: insights from grain characterisation, ring-shear tests and analogue experiments. J. Struct. Geol. 28, 1710–1724.
Schulz, B.M., Schulz, M., 2006. The dynamics of wet granular matter. J. Non-Cryst. Solids 352, 4877–4879.
Spaniol, B., Bica, V.C., Ruppenthal, L.R., Volpato, M.R., Petrovick, P.R., 2009. Compressional behavior of a mixture of granules containing high load of *Phyllanthus niruri* spray-dried extract and granules of adjuvants: comparison between eccentric and rotary tablet machines. AAPS PharmSciTech J. 10, 1013–1023.
Tousey, M.D., 2002. Optimal tablet press operation: machine versus granulation. Pharm. Technol. 26, 52–60.
Tomas, J.R., 2001. Assessment of mechanical properties of cohesive particulate solids. Part 1: Particle contact constitutive model. Partic. Sci. Technol. 19, 95–110.
Ugail, H., 2004. Spine based shape parametrisation for PDE surfaces. Computing 72, 195–204.
Wellmann, C., Lillie, C., Wriggers, P., 2008. Comparison of the macroscopic behavior of granular materials modeled by different constitutive equations on the microscale. Finite Elem. Anal. Des. 44, 259–271.
Wu, C.Y., Hancock, B.C., Mills, A., Bentham, A.C., Best, S.M., Elliott, J.A., 2008. Numerical and experimental investigation of capping mechanisms during pharmaceutical tablet compaction. Powder Technol. 181, 121–129.
Wu, C.Y., Thornton, C., Li, L.Y., 2003. Coefficients of restitution for elastoplastic oblique impacts. Adv. Powder Technol. 14, 435–448.
You, L.H., Comninos, P., Zhang, J.J., 2004. PDE blending surfaces with C2 continuity. Comput. Graph. 28, 895–906.